

Deep Learning Gaussian Processes For Computer Models with Heteroskedastic and High-Dimensional Outputs

Laura Schultz

*Department of Systems Engineering
and Operations Research
George Mason University
email: lschult2@gmu.edu*

Vadim Sokolov*

*Department of Systems Engineering
and Operations Research
George Mason University
email: vsokolov@gmu.edu*

First Draft: December, 2020
This Draft: September 5, 2022

Abstract

Deep Learning Gaussian Processes (DL-GP) are proposed as a methodology for analyzing (approximating) computer models that produce heteroskedastic and high-dimensional output. Computer simulation models have many areas of applications, including social-economic processes, agriculture, environmental, biology, engineering and physics problems. A deterministic transformation of inputs is performed by deep learning and predictions are calculated by traditional Gaussian Processes. We illustrate our methodology using a simulation of motorcycle accidents and simulations of an Ebola outbreak. Finally, we conclude with directions for future research.

1 Introduction

Computer simulation experiments have gained popularity among engineering and science disciplines for the modeling and study of complex processes, such as manufacturing design, financial forecasting, environmental, and human system interactions. Supercomputers now allow for more realistic models, such as the popular Agent-Based Models (ABMs) Banks and Hooten (2021); Auld et al. (2016, 2012), which simulate human behavior from a high-dimensional set of inputs and produce a large number of outputs. The complicating attribute of these simulators is their stochastic nature and heteroskedastic behavior, where noise levels depend upon the input variables Binois et al. (2018a);

*Corresponding author

Schmidt et al. (2011); Gelfand et al. (2004b). Common types of analysis with stochastic simulators include sensitivity analysis, prediction, optimization and calibration.

Traditional Monte Carlo-based approaches rely on repeated runs of each scenario for analysis Baker et al. (2020); however, high-dimensional state-spaces are exponentially large and render most sampling methods ineffective. Another caveat is an inability to calculate derivatives of the simulator’s input-output relationship and its stochastic nature makes formal statistical inference Moré and Wild (2009); Borgonovo et al. (2022) inapplicable in these settings. Alternatively, the Bayesian surrogate approach Sacks et al. (1989); Kennedy and O’Hagan (2001), which uses a statistical surrogate model to approximate the simulator Gramacy and Lee (2009); Snoek et al. (2014); Danielski et al. (2013); Rasmussen and Williams (2006); Romero et al. (2013), has an analytical likelihood that can be used to infer behaviors in unevaluated regions. In this paper we propose a Bayesian framework to solve the prediction problem for simulators that are high dimensional and have multiple heteroskedastic outputs.

Our Bayesian approach places a Gaussian Process (GP) prior over the simulator’s outputs and calculates the posterior using the results of initial model runs. The Bayesian approach allows for explicit quantification of uncertainty in unobserved input regions and the non-parametric GP model can learn complex input-output relations. However, the technique relies heavily on the informational contribution of each sample point and quickly becomes ineffective when faced with significant increases in dimensionality Shan and Wang (2010); Donoho (2000). Further, commonly fielded GP models assume that output variance is homogeneous. However, this assumption often proves unrealistic in practice and, therefore, the homogeneous models predict poorly Binois et al. (2018b). Unfortunately, the consideration of each input location to handle these heteroskedastic cases result in analytically intractable predictive density and marginal likelihoods Lázaro-Gredilla et al. (2010). Furthermore, the smoothness assumption made by GP models hinders capturing rapid changes and discontinuities in the input-output relations. Popular attempts to overcome these issues include relying on the selection of kernel functions using prior knowledge about the target process Cortes et al. (2004); splitting the input space into sub-regions so that inside each of those smaller subregions the target function is smooth enough and can be approximated with a GP model Gramacy and Lee (2008); Gramacy and Apley (2015); Chang et al. (2014); and learning spatial basis functions Bayarri et al. (2007); Wilson et al. (2014); Higdon (2002).

Another important feature of many practical computer models is that they have high-dimensional outputs. A naive approach to dealing with this is to place Gaussian priors to each of the outputs Conti and O’Hagan (2010). However, this approach ignores the correlation structure among the outputs, making learning less efficient Caruana (1997); Bonilla et al. (2008) and can be computationally expensive when the number of outputs is large. Another approach Gattiker et al. (2006) is to assume the Kronecker structure in the simulation outputs, but this approach has limited applicability due to the constraints it adds to the form of the GP covariance function and assumption that data is iid.

An alternative technique builds on the Linear Models of Coregionalization (LMC) approach originally used to model non-stationary and heteroskedastic spatio-temporal processes Mardia and Goodall (1993); Goulard and Voltz (1992); Gelfand et al. (2004a). A linear mixture of independent regression tasks are combined with coregionalization

matrices to capture input-output correlations Teh et al. (2005); Bonilla et al. (2008); Osborne et al. (2009). A primary advantage of this technique is the ability to use standard GPs, which assume stationary and isotropic variance, to produce a non-separable, non-stationary, and anisotropic estimation Reich et al. (2011). There are several approaches to construct such a cross-covariance function for multiple output problems. For example, Myers (1984) proposed multi-output functions which accounts for potential interdependence and use the LMC technique; Convolutional Processes (CP) have been adapted by convolving univariate regression tasks with different smoothing kernel functions Higdon (2002); Barry and Jay M. Ver Hoef (1996); Álvarez et al. (2019); while, in the field of machine learning, Multi-task GPs construct a secondary covariance function Bonilla et al. (2008); Álvarez and Lawrence (2011) between outputs. However, these approaches quickly grow unwieldy at high dimensions due to their additional correlation function in the order of $p(p+1)/2$ for p outputs. In addition, their smoothness assumptions still hinder capturing rapid slope changes and discontinuities. For a recent discussion see Genton and Kleiber (2015).

One advantage of our approach is that we extend the coregionalization technique to handle functional, heteroskedastic computer model outputs. We add a pre-processing step that uses deep learning model to transform the training data set as previously proposed Schultz and Sokolov (2018); Schultz et al. (2022); Bhadra et al. (2021); Polson et al. (2021); Nareklshvili et al. (2022); Wikle (2019); Wikle and Zammit-Mangion (2022). Our model uses deterministic transformation of the input θ defined by a deep learner $\psi = \phi(\theta)$ and then assumes that the heteroskedastic output y is a weighted sum of the basis vectors $F(\psi)$ with $F(\psi)$ being the univariate Gaussian Processes. We define an estimation procedure that jointly estimates the parameters of the deep learning transformation, the basis vectors and hyperparameters of the univariate GPs. The goal of the deterministic transformation ϕ to find a vector representation of the input sets of the parameters so that dimensionality of this representation is lower compared to dimensionality of the output. Further, the basis vectors F model correlation structure among elements of the output vector y . Further, we use an additional noise variable e assigned to each of the p outputs to account for any independent variations in the outputs. The model can now capture conditional relationships and any non-stationary and anisotropic behaviors without making the linear assumptions of other LMC methods or introducing new variable constraints Higdon (2002); Reich et al. (2011). Further, this approach explicitly captures the uncertainty in the relations between the transformed inputs ψ and the output y . By doing this, we improve our dimensionality reduction by introducing uncertainty to the latent features ψ , and further, we capture the uncertainty in the outputs y . By adding a deep learning pre-processing with Gaussian Process allows us to model discontinuities and steep slope changes.

The remainder of the paper is organized as follows. In Section 3, we outline our modelling approach in detail. In Section 4, we discuss various, limiting GP assumptions and illustrate how our model circumvents them. In Section 5, we demonstrate our approach and apply our methodology to the epidemic model data produced by a stochastic, agent-based model (ABM) used in Fadikar et al. (2018). Finally, we provide a summary and potential opportunities for future work in Section 6.

2 Background

For context, we briefly review the GP regression method for a univariate output y given observed input-output pairs $\mathcal{D} = \{\theta^{(i)}, y(\theta^{(i)})\}_{i=1}^N$. The surrogate model seeks to approximate y as follows,

$$y_i = F(\theta_i) + \epsilon(\theta) + e_i. \quad (1)$$

The error $\epsilon(\theta)$ captures any parameter uncertainty, model inadequacy, and residual variability Kennedy and O'Hagan (2001); and e represents the observation error and residual variation inherent to the true process which generates y .

Traditionally, Gaussian Process surrogates have been used for modeling F by assigning a GP prior over a space of smooth functions, then updating this prior using the observed data \mathcal{D} . The resulting posterior distribution accounts for the uncertainty at unobserved points in the domain when performing interpolation and prediction; a GP is fully characterized by its mean function m and covariance function, or kernel, k Gramacy and Polson (2011).

$$F(\theta) \sim \mathcal{GP}(m(\theta), k(\theta)), \quad (2)$$

where $k(\theta)_{ij} = k(\theta_i, \theta_j)$, $i \neq j$.

It is common to model the prior mean by setting it to zero or via regression

$$\mu(\theta) = h(\theta).$$

The correlation equation $k(\theta)$ must result in a positive semi-definite matrix; in this paper, we use the Squared Exponential kernel, which is both stationary and isotropic:

$$k_{SE}(\theta, \theta') = \exp \left[-\frac{1}{2} \left(\frac{\theta - \theta'}{\lambda} \right)^2 \right]$$

where λ represents the lengthscale hyperparameter.

General references can be found in Abrahamsen (1997) and Duvenaud (2014).

Additionally, the inadequacy errors of $\epsilon(\theta)$ in Equation 1 can be incorporated via a specialized Linear ‘‘nugget’’ $r(\theta) = \mathcal{N}(0, I\sigma_\epsilon^2)$ Gramacy and Lee (2012):

$$\mathcal{L}(\theta) \sim \mathcal{GP}(m(\theta), K(\theta) = k(\theta, \theta') + r(\theta)I) \quad (3)$$

where I represents the identity matrix.

Gaussian Process regression then infers the posterior distribution over functions on the observed data \mathcal{D} . The final density is a univariate Normal:

$$[y(\theta) \mid \mathcal{D}, \theta, \Omega] \sim \mathcal{N}(\mu, \Sigma), \quad (4)$$

where Ω are the parameters of the kernel function, and with the following summary statistics:

$$\begin{aligned} \mu &= m(\theta) + k(\theta)(K_{\mathcal{D}})^{-1}(y - m_{\mathcal{D}}) \\ \Sigma &= k(\theta, \theta) + r(\theta) - k(\theta)(K_{\mathcal{D}})^{-1}k(\theta)^T \end{aligned} \quad (5)$$

where $k(\theta) = \left(k(\theta, \theta^{(1)}), \dots, k(\theta, \theta^{(N)}) \right)^T$.

3 Deep Learning Gaussian Processes (DL-GP)

When approaching a multi-variable response problem, simply assigning a unique GP to each output may seem logical. However, the computational cost would be unmanageable in large dimensions and the potential conditional dependencies among outputs lost. We propose incorporating a non-linear extension of the projection-based methods by using a deep learner model to construct a nonlinear mapping $\phi(\theta) \rightarrow \psi$ that transforms the input vector θ into a lower-dimensional vector of latent variables $\psi \in \mathbb{R}^q, q \ll p$ so that a basic GP can be used to model the relations between ψ and y . A univariate prior $f(\cdot)$ is placed on each of these q variables. The subset of GPs are then linearly combined to produce probabilistic estimates of the simulated outputs $y \in \mathbb{R}^p$ using a now-manageable number of GPs. Our overall surrogate model is as follows

$$\psi = \phi_W(\theta) \quad (6)$$

$$F(\theta) = b + \mathcal{W}f(\phi_W(\theta)) + e \quad (7)$$

$$f_j(\psi_j) \sim \mathcal{GP}(m_j(\psi_j), K_j(\psi_j, \psi_j | \Omega)), j = 1, \dots, q \quad (8)$$

$$e_i \sim N(0, \sigma_{e_i}), i = 1, \dots, p \quad (9)$$

where $\mathcal{W} = (\mathcal{W}_1, \dots, \mathcal{W}_q)$ are the basis vectors; GPs f_j define weights over those basis vectors to represent the output y ; e represents the observational and residual errors of the true function; and ϕ is a deterministic non-linear map. For simplicity of notation, we will use ψ instead of $\phi_W(\theta)$ moving forward.

The simulated outputs then have a prior distribution of:

$$F_i(\theta) \sim \mathcal{GP}(M_i, S_i), i = 1, \dots, p$$

$$M_i = b_i + \sum_{j=1}^q \mathcal{W}_{ij} m_j(\psi_j) \quad (10)$$

$$S_i = \sum_{j=1}^q \mathcal{W}_{ij}^2 K_j$$

This prior is then integrated over the available data of N observed input-output pairs $\mathcal{D} = (\psi^{(N)}, y^{(N)})$ to compute the predictive posterior distribution for unobserved designs ψ :

$$F(\theta) | \mathcal{D}, \theta, \Omega \sim \mathcal{N}(\mu, \Sigma), \quad (11)$$

where Ω are the parameters of the kernel function, and with the following summary statistics:

$$\begin{aligned} \mu &= M(\psi) + S(\psi)[S(\psi_N) + I\sigma_e^2]^{-1}(y_N - M(\psi_N)) \\ \Sigma &= S(\psi, \psi) + e - S(\psi)[S(\psi_N) + I\sigma_e^2]^{-1}S(\psi)^T \end{aligned} \quad (12)$$

where $S(\psi) = (S(\psi, \psi^{(1)}), \dots, S(\psi, \psi^{(N)}))^T$.

The diagram below visualizes our model.

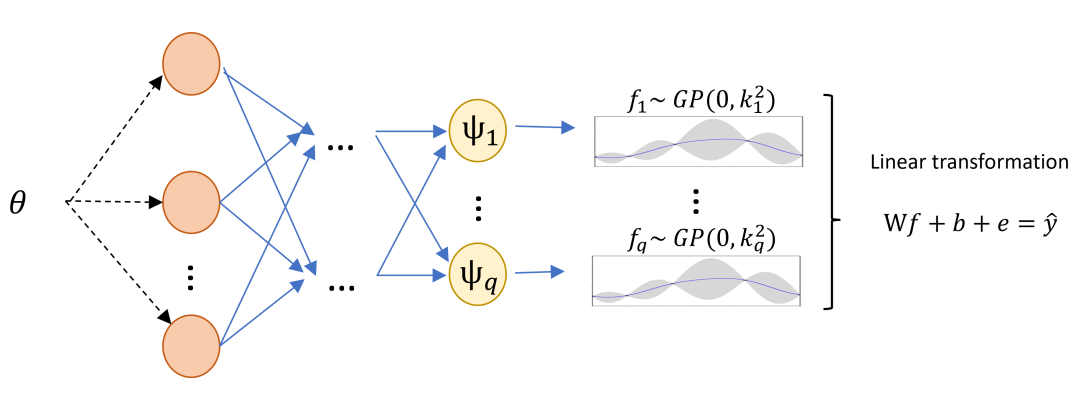


Figure 1: Visualization of the proposed DL-GP model.

The conditional density for each output now depends on the linear weighted sums of a reduced number of manageable GPs, each having unique input sets. This setup allows for conditional dependencies to be captured in the posterior for the latent GPs and shares statistical strength across outputs. Further, the separate, Gaussian error term e_i from Equation 9 allows the system’s variance unique to the particular output to be captured and allow for conditional independence.

This mixture model of latent variables is the basis of our model and analogues to the Semi-Parametric Latent Variable Model (SPLM) and Factor Analysis Model Teh et al. (2005). However, we add the additional processing step of a nonlinear projection of the latent variables.

3.1 Latent Variable Model

The quality of surrogate’s approximation depends on the quality of the training sample available. The goal is to capture the interaction behavior across the entire state-space; thereby making the placements and volume of samples critical. The volume of the input space grows exponentially as dimensionality increases. This “curse of dimensionality” leads to poor performance of non-parametric methods when inputs are high-dimensional due to the equal growth in sample volumes. Consequently, while capable of reproducing a wide range of behaviors and providing a highly flexible fit Gramacy and Polson (2011), GPs are known to fail in higher dimensions when resources are limited. Hence, we also augment the methodology with a deep learner to provide sufficient dimensionality reduction to combat sample restrictions.

Dimensional reduction is the key approach to solve the issue of high-dimensional outputs. An earlier approaches to dimensionality reduction included sparse models, which assume some local structures and that leads to a sparse covariance matrix. Another popular technique is variable selection, which choose a subset of variables providing the largest signal-to-noise ratio. However, both approaches are prone to overfitting and noise accumulation as dimensions rise Fan et al. (2014). A projection-based technique finds a

condensed representation of the dataset in a lower dimensional subspace and have traditionally been implemented due to their computational and interpretable ease. For linear instances, one may use projection-based techniques such as Principal Component Analysis (PCA) Jolliffe (2002), Partial Least Squares (PLS) Abdi (2003); Polson et al. (2021), or various single-index models Adraghi and Cook (2009).

Deep Learning networks are a class of non-linear functions which construct a predictive mapping using hierarchical layers of latent variables. The singular or multivariate output can be a continuous, discrete, or mixed value set. Each layer ℓ applies, element-wise, a univariate activation function τ to an affine transformation:

$$\begin{aligned} Z^{(1)} &= \tau^{(1)} \left(W^{(0)}\Theta + b^{(0)} \right), \\ &\dots \\ Z^{(\ell)} &= \tau^{(\ell)} \left(W^{(\ell-1)}Z^{(\ell-1)} + b^{(\ell-1)} \right), \\ \hat{Y} &= W^\ell Z^\ell + b^{(\ell)}, \end{aligned} \tag{13}$$

where W represents the weights placed on the layer's input set Z , and b represents the offset value critical to recovering shifted multivariate functions.

Given the number of layers ℓ , the multi-layered predictor is a composite map of cascading transformations

$$Y = \left(\tau_1^{W_1, b_1} \circ \dots \circ \tau_\ell^{W_\ell, b_\ell} \right) (\theta) \tag{14}$$

The general approximation capabilities of deep learning networks is rooted in the premise first outlined by Kolmogorov Kůrková (1992): any multivariate function $h(x)$ can be alternatively expressed as a finite composition of univariate functions and affine transformations¹.

This is conceptually similar to the statistical *ridge function* approximation paradigm Chui and Li (1992); Le Méhauté et al. (1997). Commonly referred to as Projection Pursuit Regression, the technique also asserts a multivariate function $h : \mathbb{R}^n \rightarrow \mathbb{R}$ can be approximately decomposed into a fixed set of q directional hyperplanes known as *ridge functions*:

$$h(\theta) = \sum_{i=1}^q g_i(a^i \cdot \theta), \tag{15}$$

where $g_i : \mathbb{R} \rightarrow \mathbb{R}$ is a transformation function and $a^i \in \mathbb{R}^n \setminus \{0\}, k < n$ is a directional matrix.

Deep learning networks can be alternatively viewed as a projection pursuit algorithm with nonlinear link functions. Each node effectively behaves as a dividing manifold and segregates the state-space collaboratively. In deep learning multi-layer networks, resultant stacking effect with each hidden layer is an exponential growth in the number of the system's dividing hyperplanes. As data progresses down the network, each layer applies a folding operator to predecessor's divided space.

¹an affine transformation is a vector of a linear transformation plus an offset constant

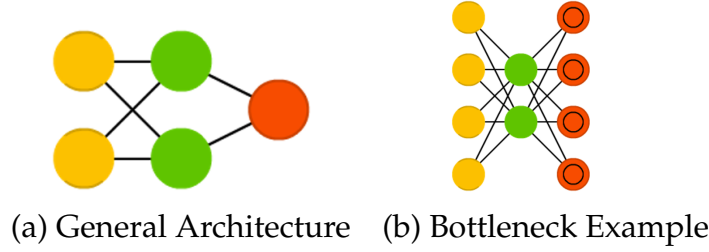


Figure 3: Each circle calculates a weighted sum of an input vector plus bias and applies a non-linear function to produce an output. Yellow and red colored neurons are input-output cells correspondingly. Source: <http://www.asimovinstitute.org/neural-network-zoo>.

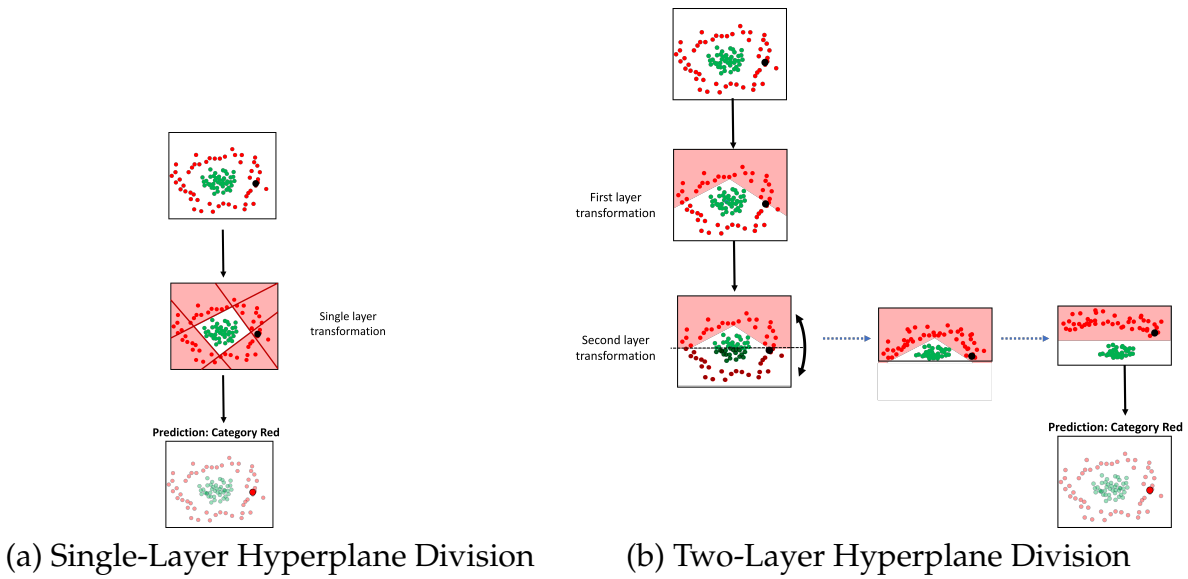


Figure 2: (a) A single layer network relies on hyperplanes (4 in this example) to partition the state space to correctly predict which group (red or green) the unknown dot (black) belongs to. (b) In a multi-layered network, each additional hidden layer allows the network to fold the developed hyperplane partitions of the previous layer independent of axis or orientation. The result is a need for less nodes in the previous layer (2 in this example) and ability to learn more complex patterns with less parameters.

As shown in Figure 2, these recursive folds produce input-space regions independent of coordinate axes and, more pointedly, of different sizes Montúfar et al. (2014); Pascanu et al. (2013) in a significantly lower number of nodes Delalleau and Bengio (2011).

Deep learning multi-layered networks designed for dimensionality reduction learning must contain at least one layer $Z^{(i)} \in \mathbb{R}^q$ with fewer nodes than the input or output layer of interest. This bottleneck layer forces the network to learn a compressed, or lower dimensional, set of latent features ψ describing the input-output relationship.

We use this representational form to extract a finite number of $q \ll p$ latent variables ψ via the last hidden deep learner layer and incorporate our linearly mixed GP model

by individually placing a univariate prior $f(\psi_j)$ on these unique feature mappings. The resulting GPs are then mixed using a final affine transformation, as documented in Equation 7.

Consequently, the error term for each single response variable psi does not correspond to the original, principal subspace of the observed data but to the strength of the nonlinear projections in accounting for simulation discrepancy sources like parameter uncertainty, model inadequacy, and residual variability Kennedy and O’Hagan (2001).

3.2 Model Estimation

Our composite model given by Equations (6) - (9) is estimated using a maximum likelihood approach. The goal is to find the parameters $\{\Omega, W, \mathcal{W}, b\}$ which best capture the given data \mathcal{D} , where Ω are the hyperparameters of the kernel functions of Gaussian processes $f_j, j = 1, \dots, q$, W are the weights of the deep learning function ϕ and \mathcal{W} is the matrix the basis vectors that approximate the y -space.

Estimating these parameters represents a non-convex optimization problem. Deep learning model parameters are typically solved through a first-order method called *gradient descent*, or *backpropagation*. The gradient of a selected measure of error ξ , such as Maximum Likelihood Error (MSE) or Cross-Entropy Error, with respect to every weight and bias is found and used to update the original weights and biases:

$$W^\ell = W^\ell - \alpha \frac{\partial \xi}{\partial W^\ell}. \quad (16)$$

Our model’s error function ξ focuses on minimizing the log marginal likelihood.

$$L(y) \propto -\frac{1}{2}y^T \left(S^{-1}y - \frac{1}{2} \log |S| - \frac{N}{2} \log(2\pi) \right) \quad (17)$$

where $F(\theta) \sim N(0, S)$.

While backpropagation can be applied to both the deep learning and mixed model weights and biases, the aggregation and resulting volatility in gradient methods do not provide satisfactory estimates for the GP hyperparameters. Particular to our paper’s example, high time-correlated signals can produce severe vanishing gradient effects and cause convergence issues in gradient descent methods Arasaratnam and Haykin (2008). Singly, GP implementations often approximate their unknown parameters through deterministic methods, such as Maximum Likelihood Estimate (MLE) or Maximum A Priori (MAP) estimates Gibbs and MacKay (1997) or Markov Chain Monte Carlo (MCMC) sampling methods, such as Gibbs or Metropolis-Hastings. This paper excludes the GP-related hyperparameters from gradient descent training and uses a more generalized Monte Carlo method known as Slice Sampling Neal (2003) at user-defined training intervals. This also allows our method to apply GPs which maintain non-Gaussian likelihoods.

The slice sampling algorithm Neal (1996) seeks to generate samples from a target distribution with density $\pi(\theta)$ by introducing a uniform auxiliary variable $u \sim \mathcal{U}(0, \pi(\theta))$. A horizontal line is drawn within $\pi(\theta)$ to define a horizontal ‘slice’ $S = \{\theta : u < \pi(\theta)\}$ and an interval I is formed by their union. A Markov chain is constructed by alternately

updating u and θ until the joint distribution $p(\theta, u) = p(u \mid \theta)p(\theta)$ becomes invariant. The auxiliary variable can then be discarded to provide only the sample of $\pi(\theta)$, the resulting marginal distribution. Note, since the target distribution $p(\theta)$ is unknown, a function $h(\theta)$ proportional to the distribution is substituted in the algorithm.

Algorithm 1 Univariate Slice Sampling Algorithm

```

1: Evaluate  $h(\theta_0)$ 
2: Draw  $u \sim \mathcal{U}(0, h(\theta_0))$  to define the horizontal "slice":  $S = \{\theta : u < h(\theta)\}$ 
3: Create a horizontal interval  $I = (L, R)$  enclosing  $\theta_0$ 
4: while true do
5:   Draw  $\theta_1 \sim \mathcal{U}(L, R)$ 
6:   Evaluate  $h(\theta_1)$ 
7:   if  $h(\theta_1) > u$  then
8:     break
9:   else
10:    modify the interval  $I$  according to a rejection procedure scheme
11:   end if
12: end while
13: return a new sample  $\theta_1$ 

```

Ideally, the interval contains as much of the slice as feasible in order to allow the new point to 'jump' or differ significantly; however, if the interval is too large in comparison with the slice, the subsequent sampling step would become less efficient. Several schemes for finding the interval exist, with the two most commonly applied being the 'stepping out' and 'doubling procedures' to shorten or lengthen the scale based on the local features of the density distribution.

In a multivariate setting, the univariate slice sampling can be applied in a one-variable-at-a-time fashion but faces difficulty with highly correlated parameters. Neal proposed a multivariate version where a hypercube bounds the target slice S . While finding the appropriate interval is done through simultaneous adjustments in all dimensions, the step-size in each dimension can be unique, allowing local behaviors by variable to be reflected automatically.

Other MCMC methods such as Gibbs sampling and Metropolis-Hastings algorithms would allow for sampling from multivariate distributions as well; however, Gibbs requires additional methods to sample from non-standard univariate distributions while Metropolis requires the user to find a precise 'proposal' distribution which can provide efficient sampling. In contrast, slice sampling avoids the need for precise tuning requirements since the algorithm's free variable, the size of the step when adjusting the sample interval, is chosen adaptively based on the local properties of the density function: if the step-size parameter is set too large, rejection procedures will exponentially tighten the interval towards the current sample while, if the value is too small, the procedures will adapt the reverse.

For this paper, we utilize the multivariate sampling method and define $h(\theta)$ as the log likelihood detailed in Equation 17.

4 Non-Smooth and Heteroskedastic Data

Although the additional nugget in Equation 3 allows us to capture stochasticity at a given point, GP models assume variable homogeneity across samples. Unfortunately, this assumption often proves unrealistic in practice but consideration of each input location to handle these heteroskedastic cases result in analytically intractable predictive density and marginal likelihoods Lázaro-Gredilla and Titsias (2011). In further complication, the corresponding assumption of Gaussian smoothness in the standard GP formulation hinders capturing rapid slope changes or discontinuities.

Handling these behaviors is typically accomplished by using kernel functions that take advantage of the structure of the underlying process Cortes et al. (2004). For example, one can split the input space into sub-regions so that inside each of those smaller sub-regions the target function is smooth enough to be approximated with a GP model Gramacy and Lee (2008); Chang et al. (2014); Kim et al. (2005). Another approach is to learn spatial bias functions Bayarri et al. (2007); Yang et al. (2015); Wilson et al. (2014); Wilson and Adams (2013); Higdon (2002). Alternatively, there are adapted GP formulations crafted to specifically model heteroskedastic data Gramacy and Polson (2011); Binois et al. (2018a); generally, the spatial relationship across points e is modeled using a secondary GP Gelfand et al. (2004a) but at the cost of an additional correlation function in the order of $p(p + 1)/2$ for p outputs.

As noted by Reich et al. (2011), the GP mixture weights of an LMC model would allow heteroskedastic behavior to be captured by automatically determining where specific feature mappings are most relevant. However, some apriori knowledge about the process is still required; for example, how many sub-regions must be captured. In our model, the deep learning multi-layered network can learn to turn certain mappings ‘on’ and ‘off’ independently of the mixture weights. Thus, we do not require any prior knowledge about the data structure. Further, the deep learning multi-layered network can transform steep slope changes into interpretable values for the GPs without introducing any linear constraints to the subspace projections Abdi (2003); Lynn and McCulloch (2000) or mixture weight restrictions like those found in Reich et al. (2011), Higdon (2002), or Teh et al. (2005).

4.1 Motorcycle Data

To illustrate, we use the heteroskedastic benchmark case detailed in Binois et al. (2018a). In addition to being non-stationary, the problem possesses similar high time-correlated noise among the inputs to our paper’s main problem. The example dataset samples the acceleration measurement y from simulated motorcycle crashes at variable times θ . Of the $N = 133$ total samples recorded, 39 use replicate inputs to capture the heteroskedastic nature of the simulation.

A visual inspection of the data in Figure 4 shows there are three regions which exhibit distinct behavior among and across samples: the left portion has a constant variance and mean; the right portion has a larger but roughly constant variance with a gentle mean change; and the middle portion contains both steep and frequent variance changes along with a volatile mean.

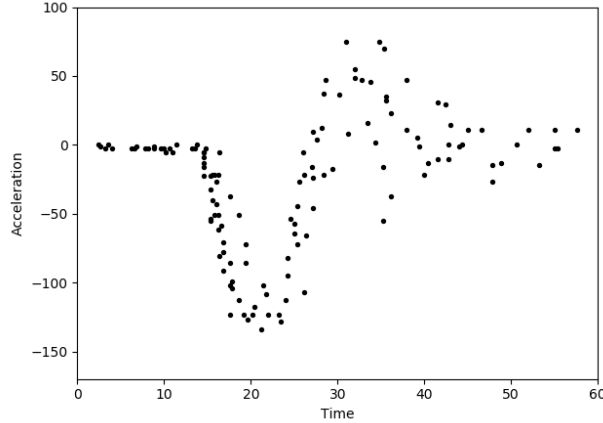


Figure 4: Motorcycle example. Black dots represent the observed data points.

In step with the methods documented in Binois et al. (2018a), we limit ourselves to a 2-dimensional GP structure and use the same Gaussian kernel to model the time-acceleration relationship. We then compare the resulting 90% Confidence Interval (CI) against the results of two relevant models: a GP-only and DL-only framework. Our first benchmark is the heteroskedastic Gaussian Process (hetGP) formulation proposed in Binois et al. (2018a). Their hetGP model produces a smoothed estimation of the nugget variable $r(\theta)$ from Equation 3 using the predictive mean of a secondary, regularizing GP. The construction of this secondary GP assumes a latent, log variation process. A joint log likelihood over both GPs allows for simultaneous optimization of all hyperparameters as well as the latent variables. For more explicit derivations, refer to Binois et al. (2018a).

For our second benchmark, we include a Deep Learning Quantile regression model, which draws from the Quantile Kriging approach established by Plumlee and Tuo (2014). For a more recent review on Quantile Kriging and its applications, see Baker et al. (2020). The model predicts 5 quantiles (0.05, 0.20, 0.5, 0.80, 0.95), or points under which a fraction of observations would fall below. For example, the 0.05 quantile should over-predict 5% of the time and contain 5% of the observations in the area beneath it. The network is trained using a combination of the the Mean Squared Error (MSE) and quantile regression loss function:

$$\frac{1}{N} \sum_{i=0}^N \left((y_i - \hat{y}_i)^2 + \max [q(\hat{y}_i - y_i), (q - 1)(\hat{y}_i - y_i)] \right) \quad (18)$$

where q is the sought quantile.

By defining the area between the .95 and .05 quantiles as the network’s predicted 90% confidence interval, the model provides a probabilistic answer despite its deterministic nature.

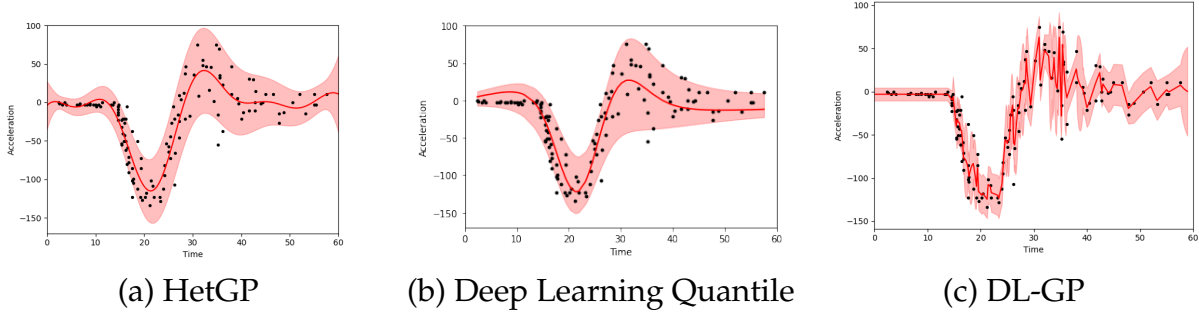


Figure 5: Motorcycle example. The model’s fitted mean is displayed as a solid red line and 90% confidence intervals are shown as red-filled regions. Black dots represent the observed data points.

The results of all three models are shown in Figure 5. As hoped, every model, to varying degrees, successfully recognizes the heteroskedastic nature of the problem. Both the Quantile and hetGP methods provide a much smoother estimate over the statespace than our DL-GP but are unable to shadow the sharp, momentary drop in speed accompanying the function’s peak like ours. In addition, our model is able to transition more rapidly to match the variance stabilization that happens on both ends of the timeline; our method is also able to reflect the nearly 90 degree drop in acceleration about the 15 second mark.

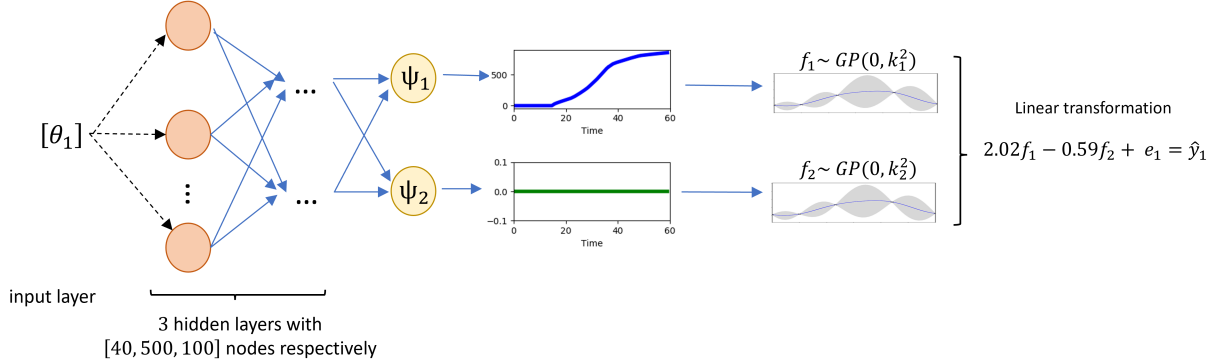


Figure 6: The deep learning model produces two unique input sets to the model’s two GPs. The first input set (blue) is variable across time while the second input set (green) remains constant. The weight (green rectangle) placed on the second GP’s output would suggest the model seeks to eliminate a homoskedastic white noise present in the observations (black dots).

Figure 6 shows how the original subspace is transformed prior to the GP layer. The first GP is provided a variable input while the second GP is given a white-noise input. The lack of input changes in the second GP suggests that the additional dimension represents a source of homoskedastic noise found in the data. The negative weight assigned to its correspondent GP suggests that the deep learning feature serves as a counter to a systemic noise source like measurement error.

For quantifiable comparison, we follow the same experimental setup of 300 independent splits generated by randomly subdividing the full dataset into 90%-10% training and testing sets. Our methodology’s performances across partitions are used to generate the Normalized Mean Squared Error (NMSE) and Negative Log-Probability Density (NLPD) metrics detailed in the original Lázaro-Gredilla and Titsias (2011) study:

$$\begin{aligned}
NMSE &= \frac{\sum_{j=1}^{n_*} (y_{*j} - \hat{y}_{*j})^2}{\sum_{j=1}^{n_*} (y_{*j} - \bar{y})^2}, \\
NLPD &= -\frac{1}{n_*} \sum_{j=1}^{n_*} \log p(y_{*j} | \mathcal{D}),
\end{aligned} \tag{19}$$

where y_{*j} is the j -th observation within the test set; \hat{y}_{*j} is the mean of the posterior for that observation; n_* is the number of test observations; and \bar{y} is the mean of the training observations.

	DL-GP	Q-DL	WHGP	GP	MAPHGP	VHGP
NMSE	0.20 ± 0.07	0.31 ± 0.21	0.28 ± 0.21	0.26 ± 0.18	0.26 ± 0.17	0.26 ± 0.17
NLPD	0.68 ± 0.18	N/A	4.26 ± 0.31	4.59 ± 0.22	4.32 ± 0.60	4.32 ± 0.30

Table 1: Average Normalized Mean Squared Error (NMSE) and Negative Log-Probability Density (NLPD) ± 1 standard deviation for 300 random partitions. Lower values are desired.

Table 1 summarizes the results for our proposed model (labeled DL-GP) and the quantile deep learner (labeled Q-DL) in comparison with those recorded in Binois et al. (2018a): their smoothed heteroskedastic GP (labeled WHGP); a standard, homoskedastic GP (labeled GP); a Maximum A Posteriori heteroskedastic GP (labeled MAPHGP) from Kersting et al. (2007); and a variational model (labeled VHGP) from Lázaro-Gredilla and Titsias (2011).

Note that our two models are comparable to these alternatives.

5 Application: Predicting Ebola Epidemic ABM

For illustration, we use the multi-output agent-based epidemic model problem documented in Fadikar et al. (2018). We predict the 56-week, simulated outputs for three holdout scenarios.

5.1 Data Set

After the 2014-2015 West Africa Ebola outbreak, the Research and Policy for Infectious Disease Dynamics (RAPIDD) program at the National Institutes of Health (NIH) convened a workshop to compile and explore the various forecasting approaches used to help

manage the outbreak. At its conclusion, a disease forecasting challenge was launched to provide 4 synthetic population datasets and scenarios as a baseline for cross-assessment. A stochastic, agent-based model Ajelli et al. (2018) first generated each population using varying degrees of data accuracy, availability, and intervention measures; individuals were then assigned activities based on demographic and survey data to model realistic disease propagation. Transmission by an infected individual is determined probabilistically based on the duration of contact with a susceptible individual and $d = 5$ static inputs $\Theta = \theta_1, \dots, \theta_5$ to the model.

Parameter	Description	Range
θ_1	probability of disease transmission	$[3 \times 10^{-5}, 8 \times 10^{-5}]$
θ_2	initial number of infected individuals	$[1, 20]$
θ_3	delay in hospital intervention	$[2, 10]$
θ_4	efficacy of hospital intervention	$[0.1, 0.8]$
θ_5	intervention reduction of travel	$[3 \times 10^{-5}, 8 \times 10^{-5}]$

Figure 7: 5 static inputs used for defining disease propagation for the Ebola ABM

A single run outputs a cumulative count of infected individuals over a 56-week period. For more details on the model and challenge, see Viboud et al. (2018).

To maintain comparison, we use the same data set from Fadikar et al. (2018), which consists of a collection of $m = 100$ scenarios generated through a space-filling, symmetric Latin hypercube design. For each scenario, 100 replicates were run for a total of $N = 10,000$ simulated epidemic trajectories. A single run for each parameter set produced a 56-dimensional output, capturing the cumulative weekly number of infected individuals. The log results for every setting combination is captured in Figure 8. For testing purposes, we exclude the same 3 unique parameter settings, which we will refer to as A, B, and C, and their respective $n = 100$ simulated outputs from the training set.

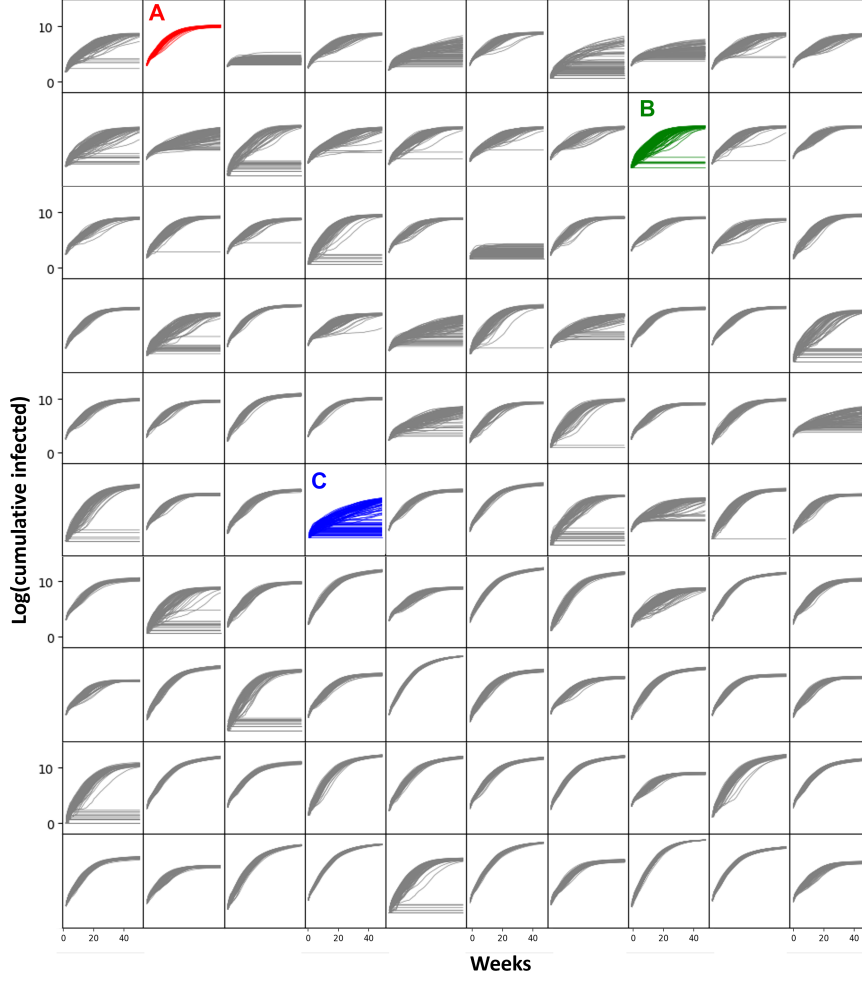


Figure 8: For each scenario, the 100 simulated trajectories for the cumulative number of disease incidences across 56 weeks are shown as grey lines. The three holdout scenarios (A, B, and C) are highlighted in red, green, and blue respectively.

Notably, different parameter settings produced strongly divergent behaviors in their replicates. Some followed a mean trajectory while others produced strong bimodal behavior, significant heteroskedasticity, or simply remained flat-lined. Fadikar et al. (2018) reasons that only a subset of replicates within each parameter settings may produce similar initial behaviors and that adding an additional variable α to index these replicates would produce more accurate predictions. Modifying the Quantile Kriging approach, the 100 replicates of each parameter setting are replaced with $n_\alpha = 5$ quantile-based trajectories. The quantiles are then indexed within each parameter set by the addition of a sixth latent variable $\alpha \in [0, 1]$:

$$\Theta = [\theta_1, \theta_2, \theta_3, \theta_4, \theta_5, \alpha]. \quad (20)$$

Figure 9 shows the 5 calculated quantiles of these three hold-out scenarios, labeled A, B, and C and highlighted in red, green, and blue respectively, that we wish to predict using our model.

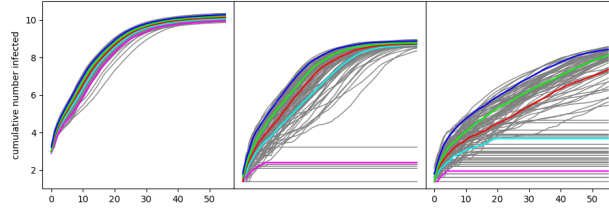


Figure 9: For each holdout scenario, labeled A, B, and C, the 100 simulated trajectories of the cumulative number of disease incidences over 56 weeks are shown as grey lines. The 5 colored lines represent the $[0.05, 0.275, 0.5, 0.725, 0.95]$ quantiles, which are now indexed by the additional sixth parameter α .

Figure 10 shows the results of our experiment. Each row of the figure corresponds to one of the holdout scenarios (A, B, and C); the first column shows the 100 replicates generated by the ABM, along with the estimated quantiles; the remaining 5 columns compare the 90% confidence intervals our model predicts for each of the 5 quantile settings estimated from the ABM replicates.

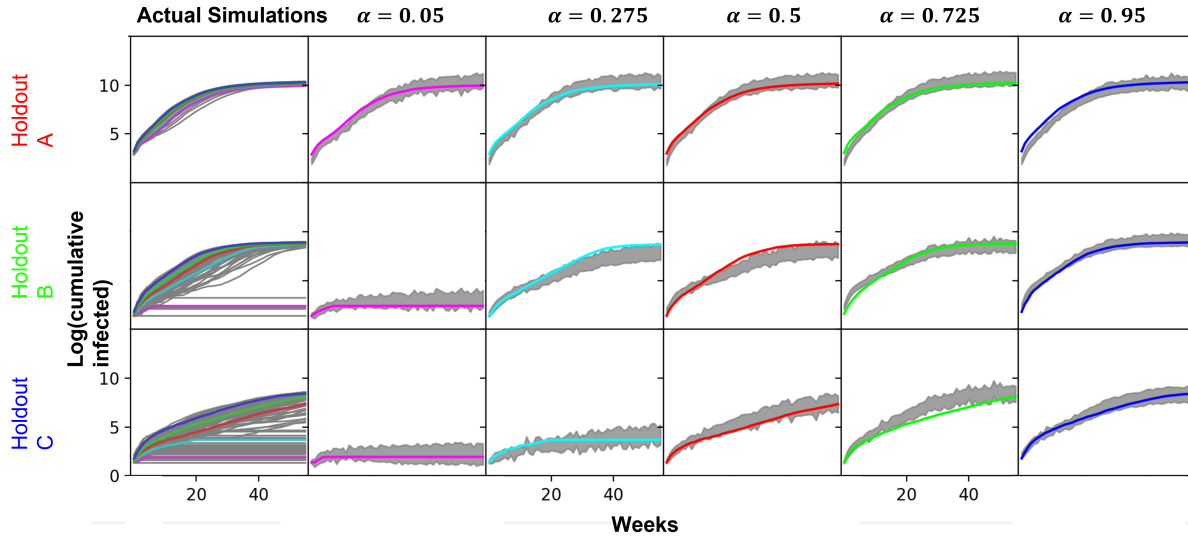


Figure 10: The first column shows the 100 actual simulations and their empirical quantiles for each of the three holdout scenarios. The next 5 columns show the predictive posterior's 90% confidence intervals for each empirical quantile, denoted by different colors.

Our model's contribution to Fadikar et al. (2017) successful approach is an improvement in capturing the saturation points of the various scenarios' disease trajectories with tighter confidence intervals, particularly during the first 20 weeks when the disease propagation is steepest, while still encompassing or closely aligning to each holdout quantile. Further, our model proves more adept at capturing the more linear growth

behaviors among several cases, though we acknowledge that the linearity in the $q = .725$ quantile for scenario C is not well captured.

Overall, our model’s predictions among the lower quantiles provide more noticeable improvements, including the correction of several of Fadikar et al. (2017) cases, to maintain the quantile across the entire timeline’s 90% CI. In contrast, some of our results underestimated the initial case loads when Fadikar et al. (2017)’s model did not; however, most of these cases incorporated the difference within the following weeks without missing the quantile’s inflection points.

6 Discussion

Deep Learning Guassian Process (DL-GP) models provide a flexible class of high-dimensional input-output models that can achieve smoothing, prediction, and calibration in a variety of contexts. Each GP is built over the significant factors found by a non-linear projection of the simulation’s inputs via a deep learning multi-layered network. This model allows us to leverage conditional relationships to help predict the outputs for high-dimensional simulators with multiple outputs without the constraints found in other methods. Furthermore, the non-linear transformation technique eliminates the unrealistic requirement of smooth, homoskedastic behavior without introducing linear constraints to the subspace projections or mixture weight restrictions. There are many directions for future research. We wish to next incorporate this new model into a calibration framework to see how it performs against our previously developed high-dimensional model, which collapsed the outputs to a single predictive value before optimizing. Additional research of interest include incorporating a parallelized or mini-batch slicing algorithm that would improve computational timing and align with the paradigm of deep learning networks training.

References

- Hervé Abdi. Partial least square regression (PLS regression). *Encyclopedia for research methods for the social sciences*, 6(4):792–795, 2003.
- Petter Abrahamsen. Gaussian random fields and correlation functions. Technical report, Technical report, Norwegian Computing Center, Oslo, Norway, 1997.
- Kofi P. Adragani and R. Dennis Cook. Sufficient dimension reduction and prediction in regression. *Philosophical Transactions of the Royal Society A: Mathematical, Physical and Engineering Sciences*, 367(1906):4385–4405, November 2009.
- Marco Ajelli, Qian Zhang, Kaiyuan Sun, Stefano Merler, Laura Fumanelli, Gerardo Chowell, Lone Simonsen, Cecile Viboud, and Alessandro Vespignani. The RAPIDD Ebola forecasting challenge: Model description and synthetic data generation. *Epidemics*, 22: 3–12, 2018.

- Mauricio A Álvarez, Wil Ward, and Cristian Guarnizo. Non-linear process convolutions for multi-output gaussian processes. In *The 22nd International Conference on Artificial Intelligence and Statistics*, pages 1969–1977. PMLR, 2019.
- Ienkaran Arasaratnam and Simon Haykin. Nonlinear Bayesian Filters for Training Recurrent Neural Networks. In Alexander Gelbukh and Eduardo F. Morales, editors, *MICAI 2008: Advances in Artificial Intelligence*, volume 5317, pages 12–33. Springer Berlin Heidelberg, Berlin, Heidelberg, 2008.
- Joshua Auld, Vadim Sokolov, Angela Fontes, and Rene Bautista. Internet-based stated response survey for no-notice emergency evacuations. *Transportation Letters*, 4(1):41–53, 2012.
- Joshua Auld, Michael Hope, Hubert Ley, Vadim Sokolov, Bo Xu, and Kuilin Zhang. Polaris: Agent-based modeling framework development and implementation for integrated travel demand and network and operations simulations. *Transportation Research Part C: Emerging Technologies*, 64:101–116, 2016.
- Evan Baker, Pierre Barbillon, Arindam Fadikar, Robert B. Gramacy, Radu Herbei, David Higdon, Jiangeng Huang, Leah R. Johnson, Pulong Ma, Anirban Mondal, Bianica Pires, Jerome Sacks, and Vadim Sokolov. Analyzing Stochastic Computer Models: A Review with Opportunities, September 2020.
- David L Banks and Mevin B Hooten. Statistical challenges in agent-based modeling. *The American Statistician*, 75(3):235–242, 2021.
- Ronald Paul Barry and Jay M. Ver Hoef. Blackbox Kriging: Spatial Prediction without Specifying Variogram Models. *Journal of Agricultural, Biological, and Environmental Statistics*, 1(3):297–322, 1996.
- Maria J Bayarri, James O Berger, Rui Paulo, Jerry Sacks, John A Cafeo, James Cavendish, Chin-Hsu Lin, and Jian Tu. A Framework for Validation of Computer Models. *Technometrics*, 49(2):138–154, May 2007.
- Anindya Bhadra, Jyotishka Datta, Nick Polson, Vadim Sokolov, and Jianeng Xu. Merging two cultures: Deep and statistical learning. *arXiv preprint arXiv:2110.11561*, 2021.
- Mickael Binois, Robert B. Gramacy, and Michael Ludkovski. Practical heteroskedastic Gaussian process modeling for large simulation experiments. *Journal of Computational and Graphical Statistics*, 27(4):808–821, October 2018a.
- Mickael Binois, Robert B Gramacy, and Mike Ludkovski. Practical heteroscedastic gaussian process modeling for large simulation experiments. *Journal of Computational and Graphical Statistics*, 27(4):808–821, 2018b.
- Edwin V Bonilla, Kian Ming A Chai, and Christopher K I Williams. Multi-task Gaussian Process Prediction. *Advances in neural information processing systems*, page 8, 2008.

- Emanuele Borgonovo, Genyuan Li, John Barr, Elmar Plischke, and Herschel Rabitz. Global Sensitivity Analysis with Mixtures: A Generalized Functional ANOVA Approach. *Risk Analysis*, 42(2):304–333, 2022.
- Rich Caruana. Multitask Learning. *Machine Learning*, 28(1):41–75, July 1997.
- Won Chang, Murali Haran, Roman Olson, and Klaus Keller. Fast dimension-reduced climate model calibration and the effect of data aggregation. *The Annals of Applied Statistics*, 8(2):649–673, June 2014.
- Charles K Chui and Xin Li. Approximation by ridge functions and neural networks with one hidden layer. *Journal of Approximation Theory*, 70(2):131–141, August 1992.
- Stefano Conti and Anthony O’Hagan. Bayesian emulation of complex multi-output and dynamic computer models. *Journal of statistical planning and inference*, 140(3):640–651, 2010.
- Corinna Cortes, Patrick Haffner, and Mehryar Mohri. Rational kernels: Theory and algorithms. *Journal of Machine Learning Research*, 5(Aug):1035–1062, 2004.
- C. Danielski, T. Kacprzak, G. Tinetti, and P. Jagoda. Gaussian Process for star and planet characterisation. *arXiv:1304.6673 [astro-ph]*, April 2013.
- Olivier Delalleau and Yoshua Bengio. Shallow vs. Deep Sum-Product Networks. In J. Shawe-Taylor, R. S. Zemel, P. L. Bartlett, F. Pereira, and K. Q. Weinberger, editors, *Advances in Neural Information Processing Systems 24*, pages 666–674. Curran Associates, Inc., 2011.
- David L. Donoho. High-dimensional data analysis: The curses and blessings of dimensionality. In *Ams Conference on Math Challenges of the 21st Century*, 2000.
- David Duvenaud. *Automatic model construction with Gaussian processes*. PhD thesis, University of Cambridge, 2014.
- Arindam Fadikar, Dave Higdon, Jiangzhuo Chen, Brian Lewis, Srini Venkatramanan, and Madhav Marathe. Calibrating a Stochastic Agent Based Model Using Quantile-based Emulation. *arXiv:1712.00546 [stat]*, December 2017.
- Arindam Fadikar, Dave Higdon, Jiangzhuo Chen, Bryan Lewis, Srinivasan Venkatramanan, and Madhav Marathe. Calibrating a stochastic, agent-based model using quantile-based emulation. *SIAM/ASA Journal on Uncertainty Quantification*, 6(4):1685–1706, 2018.
- Jianqing Fan, Fang Han, and Han Liu. Challenges of Big Data Analysis. *National science review*, 1(2):293–314, June 2014.
- Jim Gattiker, Dave Higdon, Sallie Keller-McNulty, Michael McKay, Leslie Moore, and Brian Williams. Combining experimental data and computer simulations, with an application to flyer plate experiments. *Bayesian Analysis*, 1(4):765–792, 2006.

- Alan E. Gelfand, Alexandra M. Schmidt, Sudipto Banerjee, and C. F. Sirmans. Nonstationary multivariate process modeling through spatially varying coregionalization. *Test*, 13(2):263–312, December 2004a.
- Alan E Gelfand, Alexandra M Schmidt, Sudipto Banerjee, and CF Sirmans. Nonstationary multivariate process modeling through spatially varying coregionalization. *Test*, 13(2): 263–312, 2004b.
- Marc G Genton and William Kleiber. Cross-covariance functions for multivariate geostatistics. *Statistical Science*, 30(2):147–163, 2015.
- Mark Gibbs and David J. C. MacKay. Efficient Implementation of Gaussian Processes. Technical report, Cavendish Laboratory, Cambridge, 1997.
- Michel Goulard and Marc Voltz. Linear coregionalization model: tools for estimation and choice of cross-variogram matrix. *Mathematical Geology*, 24(3):269–286, 1992.
- Robert B. Gramacy and Daniel W. Apley. Local Gaussian Process Approximation for Large Computer Experiments. *Journal of Computational and Graphical Statistics*, 24(2): 561–578, April 2015.
- Robert B Gramacy and Herbert K. H Lee. Bayesian Treed Gaussian Process Models With an Application to Computer Modeling. *Journal of the American Statistical Association*, 103(483):1119–1130, September 2008.
- Robert B. Gramacy and Herbert K. H. Lee. Adaptive Design and Analysis of Supercomputer Experiments. *Technometrics*, 51(2):130–145, May 2009.
- Robert B. Gramacy and Herbert K. H. Lee. Cases for the nugget in modeling computer experiments. *Statistics and Computing*, 22(3):713–722, May 2012.
- Robert B. Gramacy and Nicholas G. Polson. Particle Learning of Gaussian Process Models for Sequential Design and Optimization. *Journal of Computational and Graphical Statistics*, 20(1):102–118, January 2011.
- Dave Higdon. Space and space-time modeling using process convolutions. In *Quantitative methods for current environmental issues*, pages 37–56. Springer, 2002.
- I. Jolliffe. *Principal Component Analysis*. Springer New York, 2 edition, 2002.
- Marc C. Kennedy and Anthony O’Hagan. Bayesian calibration of computer models. *Journal of the Royal Statistical Society: Series B (Statistical Methodology)*, 63(3):425–464, January 2001.
- Kristian Kersting, Christian Plagemann, Patrick Pfaff, and Wolfram Burgard. Most Likely Heteroscedastic Gaussian Process Regression. In *Proceedings of the 24th International Conference on Machine Learning, ICML ’07*, pages 393–400, New York, NY, USA, 2007. Association for Computing Machinery.

- Hyoung-Moon Kim, Bani K. Mallick, and C. C. Holmes. Analyzing Nonstationary Spatial Data Using Piecewise Gaussian Processes. *Journal of the American Statistical Association*, 100(470):653–668, June 2005.
- Věra Kůrková. Kolmogorov’s theorem and multilayer neural networks. *Neural Networks*, 5(3):501–506, January 1992.
- Miguel Lázaro-Gredilla and Michalis K Titsias. Variational heteroscedastic gaussian process regression. In *ICML*, 2011.
- Miguel Lázaro-Gredilla, Joaquin Quinonero-Candela, Carl Edward Rasmussen, and Aníbal R Figueiras-Vidal. Sparse spectrum gaussian process regression. *The Journal of Machine Learning Research*, 11:1865–1881, 2010.
- Alain Le Méhauté, Christophe Rabut, and Larry L. Schumaker, editors. *Surface fitting and multiresolution methods*. Vanderbilt University Press, Nashville, TN, 1st ed edition, 1997.
- Henry S. Lynn and Charles E. McCulloch. Using Principal Component Analysis and Correspondence Analysis for Estimation in Latent Variable Models. *Journal of the American Statistical Association*, 95(450):561–572, 2000.
- Kanti V Mardia and Colin R Goodall. Spatial-temporal analysis of multivariate environmental monitoring data. *Multivariate environmental statistics*, 6(76):347–385, 1993.
- Guido Montúfar, Razvan Pascanu, Kyunghyun Cho, and Yoshua Bengio. On the Number of Linear Regions of Deep Neural Networks. *arXiv e-prints*, page arXiv:1402.1869, February 2014.
- Jorge J Moré and Stefan M Wild. Benchmarking derivative-free optimization algorithms. *SIAM Journal on Optimization*, 20(1):172–191, 2009.
- Donald E. Myers. Co-Kriging — New Developments. In Georges Verly, Michel David, Andre G. Journel, and Alain Marechal, editors, *Geostatistics for Natural Resources Characterization: Part 1*, pages 295–305. Springer Netherlands, Dordrecht, 1984.
- Maria Nareklishvili, Nicholas Polson, and Vadim Sokolov. Deep partial least squares for iv regression. *arXiv preprint arXiv:2207.02612*, 2022.
- Radford M. Neal. *Bayesian Learning for Neural Networks*, volume 118 of *Lecture Notes in Statistics*. Springer New York, New York, NY, 1996.
- Radford M Neal. Slice sampling. *The annals of statistics*, 31(3):705–767, 2003.
- Michael A Osborne, Roman Garnett, and Stephen J Roberts. Gaussian processes for global optimization. In *3rd international conference on learning and intelligent optimization (LION3)*, pages 1–15. Citeseer, 2009.
- Razvan Pascanu, Guido Montufar, and Yoshua Bengio. On the number of response regions of deep feed forward networks with piece-wise linear activations. *arXiv:1312.6098 [cs]*, December 2013.

- Matthew Plumlee and Rui Tuo. Building accurate emulators for stochastic simulations via quantile kriging. *Technometrics*, 56(4):466–473, 2014.
- Nicholas Polson, Vadim Sokolov, and Jianeng Xu. Deep learning partial least squares. *arXiv preprint arXiv:2106.14085*, 2021.
- Carl Edward Rasmussen and Christopher K. I. Williams. *Gaussian processes for machine learning*. Adaptive computation and machine learning. MIT Press, Cambridge, Mass, 2006.
- Brian J. Reich, Jo Eidsvik, Michele Guindani, Amy J. Nail, and Alexandra M. Schmidt. A class of covariate-dependent spatiotemporal covariance functions for the analysis of daily ozone concentration. *Annals of Applied Statistics*, 5(4):2425–2447, 2011.
- Philip A. Romero, Andreas Krause, and Frances H. Arnold. Navigating the protein fitness landscape with Gaussian processes. *Proceedings of the National Academy of Sciences*, 110(3):E193–E201, 2013.
- Jerome Sacks, William J. Welch, Toby J. Mitchell, and Henry P Wynn. Design and Analysis of Computer Experiments. *Statistical Science*, 4(4):409–423, November 1989.
- Alexandra M. Schmidt, Peter Guttorp, and Anthony O’Hagan. Considering covariates in the covariance structure of spatial processes. *Environmetrics*, 22(4):487–500, June 2011.
- Laura Schultz and Vadim Sokolov. Bayesian Optimization for Transportation Simulators. *Procedia Computer Science*, 130:973–978, 2018.
- Laura Schultz, Joshua Auld, and Vadim Sokolov. Bayesian calibration for activity based models. *arXiv preprint arXiv:2203.04414*, 2022.
- Songqing Shan and G. Gary Wang. Survey of modeling and optimization strategies to solve high-dimensional design problems with computationally-expensive black-box functions. *Structural and Multidisciplinary Optimization*, 41(2):219–241, March 2010.
- Jasper Snoek, Kevin Swersky, Richard S. Zemel, and Ryan P. Adams. Input Warping for Bayesian Optimization of Non-Stationary Functions. In *ICML*, pages 1674–1682, 2014.
- Yee Whye Teh, Matthias Seeger, and Michael I Jordan. Semiparametric latent factor models. In *International Workshop on Artificial Intelligence and Statistics*, pages 333–340. PMLR, 2005.
- Cécile Viboud, Kaiyuan Sun, Robert Gaffey, Marco Ajelli, Laura Fumanelli, Stefano Merler, Qian Zhang, Gerardo Chowell, Lone Simonsen, and Alessandro Vespignani. The RAPIDD ebola forecasting challenge: Synthesis and lessons learnt. *Epidemics*, 22:13 – 21, 2018.
- Christopher K Wikle. Comparison of deep neural networks and deep hierarchical models for spatio-temporal data. *Journal of Agricultural, Biological and Environmental Statistics*, 24(2):175–203, 2019.

- Christopher K Wikle and Andrew Zammit-Mangion. Statistical deep learning for spatial and spatio-temporal data. *arXiv preprint arXiv:2206.02218*, 2022.
- Andrew Wilson and Ryan Adams. Gaussian process kernels for pattern discovery and extrapolation. In *International conference on machine learning*, pages 1067–1075. PMLR, 2013.
- Andrew G Wilson, Elad Gilboa, Arye Nehorai, and John P Cunningham. Fast kernel learning for multidimensional pattern extrapolation. *Advances in neural information processing systems*, 27, 2014.
- Wen-Hsi Yang, Christopher K. Wikle, Scott H. Holan, D. Brenton Myers, and Kenneth A. Sudduth. Bayesian Analysis Of Spatially-Dependent Functional Responses With Spatially-Dependent Multi-Dimensional Functional Predictors. *Statistica Sinica*, 25(1):205–223, 2015.
- Mauricio A. Álvarez and Neil D. Lawrence. Computationally efficient convolved multiple output Gaussian processes. *Journal of Machine Learning Research*, 12(May):1459–1500, 2011.